Positioning of chemosensory proteins and FtsZ through the *Rhodobacter sphaeroides* cell cycle

Sheng-Wen Chiu,[1] Mark A. J. Roberts,[1,2†] Mark C. Leake[3] and Judith P. Armitage[1,2*]

[1]Department of Biochemistry, University of Oxford, Oxford OX1 3QU, UK; [2]Oxford Centre for Integrative Systems Biology, University of Oxford, Oxford OX1 3QU, UK; [3] Departments of Physics and Biology, University of York, York YO10 5DD, UK.

[*]For correspondence. E-mail judith.armitage@bioch.ox.ac.uk; Tel. 01865613293; Fax 01865613338. †Present address: Barts and The London School of Medicine & Dentistry, Queen Mary, University of London, London E1 2AD, UK. Author contributions: SWC, MAJR, MCL, and JPA conceived the research and designed the experiments; SWC performed the experiments; SWC, MAJR, MCL, and JPA analyzed the data and wrote the paper.

Running title: Choreography of chemosensory proteins and FtsZ

This article has been accepted for publication and undergone full peer review but has not been through the copyediting, typesetting, pagination and proofreading process, which may lead to differences between this version and the Version of Record. Please cite this article as doi: 10.1111/mmi.12366

[Keywords: chemotaxis protein cluster localization / FtsZ / MreB / ParA / polarity / *Rhodobacter sphaeroides*]

Summary

Bacterial chemotaxis depends on signaling through large protein complexes. Each cell must inherit a complex on division, suggesting some coordination with cell division. In *Escherichia coli* the membrane-spanning chemosensory complexes are polar and new static complexes form at pre-cytokinetic sites, ensuring positioning at the new pole after division and suggesting a role for the bacterial cytoskeleton. *Rhodobacter sphaeroides* has both membrane-associated and cytoplasmic, chromosome-associated chemosensory complexes. We followed the relative positions of the two chemosensory complexes, FtsZ and MreB in aerobic or photoheterotrophic *R. sphaeroides* cells using fluorescence microscopy. FtsZ forms polar spots after cytokinesis, which redistribute to the midcell forming nodes from which FtsZ extends circumferentially to form the Z-ring. Membrane-associated chemosensory proteins form a number of dynamic unit-clusters with mature clusters containing about 1000 $CheW_3$ proteins. Individual clusters diffuse randomly within the membrane, accumulating at new poles after division but not colocalizing with either FtsZ or MreB. The cytoplasmic complex colocalizes with FtsZ at midcells in new-born cells. Before cytokinesis one complex moves to a daughter cell, followed by the second

moving to the other cell. These data indicate that two homologous complexes use different mechanisms to ensure partitioning, and neither complex utilizes FtsZ or MreB for positioning.

Introduction

Recent advances in bacterial cell biology have dramatically increased our appreciation of the exquisitely organized and dynamic subcellular architecture of bacterial cells (Gitai, 2005). Many macromolecular complexes occupy specific subcellular locations and exhibit dynamic behaviors (Govindarajan *et al.*, 2012; Rudner and Losick, 2010), therefore, understanding spatial dynamics is essential to understand biological processes in bacteria. Chemotaxis and cell division are very different cellular activities but both are accomplished by the concerted actions of several molecular complexes that localize at specific sites in the cell (de Boer, 2010; Sourjik and Armitage, 2010). At cell division each daughter cell must inherit a complement of chemosensory proteins to allow efficient chemotaxis, meaning positioning of the chemosensory proteins must coordinate with cell division and it has been suggested that sophisticated mechanisms have evolved to orchestrate the spatial regulation of cell division and chemotaxis (Ringgaard *et al.*, 2011; Sourjik and Armitage, 2010).

Chemotaxis is one of the best-studied model systems of signal transduction. The *Escherichia coli* chemotactic machinery has been extensively characterized (Sourjik and Armitage, 2010; Sourjik and Wingreen, 2012). The chemotaxis pathway starts

with transmembrane chemoreceptors, which detect chemoeffectors and transmit signals to regulate the autophosphorylation of the cytoplasmic histidine kinase, CheA. The adaptor CheW facilitates the interactions between CheA and receptors. CheA transfers phosphoryl groups to the response regulator CheY. CheY-P released from the receptor complex diffuses to the flagellar motor and promotes a switch in the rotational direction of flagella (Sourjik and Armitage, 2010; Sourjik and Wingreen, 2012). Thousands of chemosensory proteins, including receptors, CheA, and CheW, form large membrane clusters at the cell poles and smaller clusters along the cell body (Briegel *et al.*, 2009; Sourjik and Armitage, 2010). Fluorescence microscopy and cryo-electron tomography suggest a preferential polar/subpolar localization of these clusters in bacterial species studied so far (Briegel *et al.*, 2009; Porter *et al.*, 2011; Sourjik and Armitage, 2010).

Three mechanisms have been proposed for the polar localization of membrane chemosensory clusters mainly based on the studies of *E. coli* and *Vibrio cholerae*. The stochastic self-assembly model suggests newly synthesized proteins either join existing clusters or nucleate new ones (Greenfield *et al.*, 2009; Thiem and Sourjik, 2008; Wang *et al.*, 2008). In this model, cluster nucleation is distance-dependent and away from existing clusters. This results in a periodic distribution of clusters along the cell body, with the cluster size decreasing in the order of old-pole, new-pole, midcell,

quarters, and so on. This mechanism ensures an even partitioning of membrane chemosensory clusters during cell division (Greenfield *et al.*, 2009; Thiem and Sourjik, 2008; Wang *et al.*, 2008). Cluster partitioning may involve anchoring the lateral clusters to pre-cytokinetic sites such that they are at new poles after cytokinesis (Thiem *et al.*, 2007). Movement of polar clusters is also restricted by unknown mechanisms, possibly the specific membrane curvature or lipid composition of the cell pole (Rudner and Losick, 2010). An alternative helical insertion diffusion-capture model suggests that newly synthesized chemoreceptors are inserted in the membrane in a helical fashion (Shiomi *et al.*, 2006), and then migrate to and form large clusters at the poles. A third ParC-mediated diffusion-capture model occurs in some polar-flagellated bacteria where a ParA homologue (see below), ParC, has a cell cycle-dependent, unipolar to bipolar localization pattern (Ringgaard *et al.*, 2011; Yamaichi, *et al.*, 2012). ParC actively recruits chemosensory proteins to the cell poles before cytokinesis, ensuring every new-born cell has an old-pole cluster after cell division.

The chemosensory systems in the α-proteobacterium *Rhodobacter sphaeroides* represent a higher level of complexity, reflecting its physiological versatility (Porter *et al.*, 2008; Porter *et al.*, 2011; Sourjik and Armitage, 2010). It is an emerging model organism for studying signal transduction complexity found in many bacteria and

more complex cells (Porter *et al.*, 2011). *R. sphaeroides* has three major operons encoding chemosensory proteins, two of which are expressed under laboratory conditions. The chemosensory proteins of these two pathways form an *E. coli*-like conventional membrane-associated pathway with membrane-spanning chemoreceptors (Mcps), and a second novel cytoplasmic pathway with soluble chemoreceptors (***t***ransducer-***l***ike ***p***roteins, Tlps) (Porter *et al.*, 2008; Porter *et al.*, 2011; Sourjik and Armitage, 2010). *R. sphaeroides* requires both pathways for chemotaxis. Separation of chemosensory proteins may enable tuning of responses to independently sensed external and internal conditions. The metabolic versatility of *R. sphaeroides* is also accompanied by the differentiation of cell morphology and subcellular architecture (Mackenzie *et al.*, 2007; Slovak *et al.*, 2005). When growing photoheterotrophically, *R. sphaeroides* develops numerous invaginations of the cytoplasmic membrane (Niederman, 2006; Niederman, 2010; Tucker *et al.*, 2010), and change their morphology from rod-shape to coccobacillus (Slovak *et al.*, 2005). The dramatic rearrangements of the cytoplasmic membrane pose a great challenge for maintaining subcellular architecture. The eukaryote-like behavior of intracytoplasmic photosynthetic membrane (Niederman, 2010) makes *R. sphaeroides* a promising model to study spatial regulation of membrane proteins during membrane differentiation.

The cytoplasmic chemosensory receptors localize as clusters at the *R. sphaeroides* midcell. After duplication, clusters appear equi-positioned (Thompson *et al.*, 2006), a pattern reminiscent of that seen for certain plasmids (Gerdes *et al.*, 2010; Lutkenhaus, 2012). Partitioning of cytoplasmic chemosensory clusters requires homologues of plasmid and chromosome DNA partitioning proteins PpfA (ParA homologue) and TlpT (ParB analog), probably using the nucleoid as a platform to ensure daughter cells each inherit a cytoplasmic cluster (Roberts *et al.*, 2012; Thompson *et al.*, 2006). There is growing evidence that ParA homologues are involved in the spatial regulation of several other protein complexes, including polar membrane chemosensory clusters in certain bacterial species (Lutkenhaus, 2012). Strikingly, current studies demonstrate an important role of the nucleoid in ParA-mediated plasmid and protein complex partitioning (Gerdes *et al.*, 2010; Jain *et al.*, 2012; Lutkenhaus, 2012; Roberts *et al.*, 2012), making it possible that the partitioning of cytoplasmic chemosensory clusters is coordinated with cell division.

The tubulin homologue FtsZ is the most critical component of the bacterial cytokinetic machinery (divisome) (Adams and Errington, 2009; de Boer, 2010; Erickson *et al.*, 2010). FtsZ is found in nearly all bacteria, many archea, and chloroplasts. FtsZ forms a ring-like structure (the Z-ring) at cytokinetic sites to establish a scaffold that sequentially recruits other divisome members, then constricts

to initiate cytokinesis. *In vitro*, FtsZ subunits assemble into protofilaments that can form higher-order structures (Erickson *et al.*, 2010). However, the *in vivo* ultra-structure of the Z-ring is still unclear. The formation and positioning of the Z-ring is coordinated with chromosome movement (Adams and Errington, 2009; de Boer, 2010; Erickson *et al.*, 2010; Thanbichler and Shapiro, 2006). In addition to FtsZ, most rod-shape bacteria contain the actin homologue MreB (Shaevitz and Gitai, 2010). MreB in *R. sphaeroides* localizes to the midcell, moving to quarter positions before the next round of cytokinesis (Slovak *et al.*, 2005).

Previous studies have suggested that chemosensory proteins in different species may use FtsZ, MreB or ParA-like systems to position the membrane cluster at cytokinetic sites or at specific poles. Our previous data have indicated that a ParA-like system positions the cytoplasmic cluster of *R. sphaeroides* to the chromosome and suggested connections between the cytokinetic site and the spatial regulation of cytoplasmic chemosensory clusters. Here, we studied the localization of FtsZ, MreB and the two chemosensory clusters in *R. sphaeroides* relative to each other during the cell cycle under different growth conditions. We found that FtsZ moves from the new pole to the midcell after cell division and, unlike *E. coli,* the membrane chemosensory clusters do not colocalize with FtsZ, but form large diffusing dynamic complexes in the membrane. Our data also suggest that these large chemosensory complexes are

composed of unit-clusters. The cytoplasmic chemosensory clusters show more defined positioning, but again are independent of both FtsZ and MreB. Despite the considerable knowledge about FtsZ accumulated during the past two decades, it is still unclear how the Z-ring forms. This study also allowed us to develop a model for Z-ring formation in *R. sphaeroides*, which may be applicable to other bacteria.

Results

Spatiotemporal dynamics of FtsZ during the cell cycle of R. sphaeroides

The spatiotemporal dynamics of FtsZ in *R. sphaeroides* have not been previously reported. We therefore characterized localization patterns of FtsZ before examining its positioning relative to chemosensory clusters. Since fluorescent protein-fusions of FtsZ homologues are not fully functional in any bacterial species studied so far (Erickson *et al.*, 2010), FtsZ was examined in a wild-type strain containing a low-copy inducible plasmid expressing *ftsZ–yfp* (yellow fluorescent protein). Leaky expression or induction with IPTG (isopropyl-β-D-thiogalactopyranoside) up to 10 μM did not affect cell growth and morphology. The typical ring-like structures (Fig. 1A, 0') were seen (Table S1). Depending on the cell-cycle stage, the Z-ring was not always a continuous, uniform structure, but frequently showed gaps (Fig. S1A) and heterogeneous distributions (Fig. S1B), consistent with current super-resolution imaging studies (Fu *et al.*, 2010; Strauss *et al.*, 2012). The midcell Z-ring constricted and further invagination produced a pair of daughter cells sharing an FtsZ assembly. The completion of septation split the shared assembly into two independent spots localized at the new poles of the two cells (Fig. 1A, 30' to 90'), similar to the cell

cycle-specific pattern seen in *Caulobacter crescentus* (Aaron *et al.*, 2007; Thanbichler and Shapiro, 2006).

A controversial aspect of current models of Z-ring constriction is whether or not FtsZ disassembles extensively and delocalizes from the Z-ring (Erickson *et al.*, 2010; Lan *et al.*, 2009; Strauss *et al.*, 2012). Quantifying time-lapse images of dividing *R. sphaeroides* cells (n=12) showed constant total intensity (0.98±0.05 fold-change [mean, with standard deviation used throughout]) of the Z-ring during constriction (from 0 to ~40% decrease in the Z-ring radius), while the Z-ring density increased (12.8±0.8% per 10% decrease in the Z-ring radius), suggesting the protein content remaining constant. The condensation of the Z-ring may provide contractile force for cytokinesis (Lan *et al.*, 2009; Strauss *et al.*, 2012).

We frequently observed noticeable differences in the intensities of FtsZ polar spots in sibling cells (Fig. 1A 90' and 1Bi 30'). The relative intensities of polar chemosensory clusters can be used to distinguish between old and young poles (Ping *et al.*, 2008). We followed the intensities of both FtsZ assemblies and polar chemosensory clusters through cell division (n=20 cell pairs) and found that in 70% (p-value=0.0184) the sibling cells with smaller polar chemosensory clusters (i.e. younger poles) received more FtsZ molecules after cytokinesis (1.89±0.56 fold, p<0.00003). This result suggests that although FtsZ content does not link to the

"absolute age" of cell poles, FtsZ may have asymmetric inheritance correlated to cellular asymmetry/polarity (Hallez *et al.*, 2004; Macara and Mili, 2008).

The development of the Z-ring

It is unclear how the Z-ring forms (Adams and Errington, 2009; de Boer, 2010; Erickson *et al.*, 2010). After cytokinesis, the polar FtsZ spots redistributed to the midcell and transverse FtsZ spatial gradients extended from the spots (Fig. 1B, i). The transverse FtsZ spatial gradients gradually encircled the midcell plane (Fig. 1B, ii). In late-septation and new-born cells FtsZ spots and short fragments were often (Table S1) visible at the future cytokinetic sites (white arrowheads, Fig. S2A), suggesting they are Z-ring precursors. Patterns of spots/fragments at the midcell periphery and time-lapse imaging suggested the Z-ring developed from these precursors, and these precursors were derived from polar spots that had moved to the midcell (Fig. 1B and S2B). The distribution of FtsZ along the precursor fluctuated before reaching a more symmetric arrangement (Fig. 1C). Intriguingly, the development process reversed in 15.85% cells (Fig. 1B, i, 60'–90', right cell; S2C). This reverse was not seen for extensively constricted Z-rings, suggesting the development process cannot reverse

once the Z-ring matures or constriction has started. The translation inhibitor chloramphenicol has no apparent effect on Z-ring development (Table S1). By quantifying YFP intensity, we found that midcell nodes/Z-ring precursors and mature Z-rings contained a larger percentage of the total FtsZ–YFP molecules than polar spots (Table S1). However, there is a significant pool of FtsZ–YFP molecules that are not localized to visible assemblies at any given time in the cell.

Therefore FtsZ forms at least two kinds of subcellular structures through the *R. sphaeroides* cell cycle: spots and ring-like assemblies. Right after cytokinesis, FtsZ assembles into polar spots which then gradually redistribute to the midcell and may have dynamic localization before Z-ring formation. The Z-ring appears to initiate at midcell precursor "nodes" (Fig. 1D), from which an FtsZ spatial gradient extends circumferentially. Initially, an asymmetric distribution of FtsZ exists but it eventually encircles the midcell plane with a more symmetric distribution. A correlation was found between the density of Z-ring/ring-precursors and total cellular intensity, but not for polar spots (Fig. S2D). These results suggest that the Z-ring becomes more dense with increasing FtsZ content, in agreement with a loose bundle model (Fu *et al.*, 2010), while the polar spot has a more constant packing density. Hence, polar spots and Z-ring/ring-precursors may have different molecular architectures.

Prior to the formation of mature Z-rings, FtsZ spots are mobile and dynamic over

our observation time scale of tens of minutes (Fig. 2). FtsZ spots were able to localize at both cell poles in the same cell (Fig. 2A, yellow arrowheads), raising the question of how FtsZ is positioned in *R. sphaeroides*. FtsZ spots appeared to integrate/separate and adjust positions (Fig. 2B), resulting in changes in spot intensity (Fig. 2). Due to the resolution limit we could not exclude the possibility that two spots came too close to be distinguished (Fig. 2B, 20'). However, the change in relative intensity (Fig. 2B, 10' to 30') suggests they integrated and reformed. This observation indicates that in *R. sphaeroides* FtsZ is repositioned to future cytokinetic sites via dynamic clusters rather than spiral structures proposed for other bacteria (Ben-Yehuda and Losick, 2002; Peters *et al.*, 2007; Specht *et al.*, 2013; Thanbichler and Shapiro, 2006; Thanedar and Margolin, 2004). However, we cannot exclude the possibility that other configurations of FtsZ assemblies may contribute to Z-ring formation in *R. sphaeroides*.

Strikingly, FtsZ has similar behaviors in photoheterotrophic cells (Fig. S3), suggesting that the dramatic rearrangement of the cytoplasmic membrane and the change in cell shape which occur during photoheterotrophic growth have no effect on the positioning of FtsZ and the cell division machinery.

Membrane chemosensory protein clusters do not localize at pre-cytokinetic sites

The stochastic self-assembly model for chemosensory clusters predicts that periodic localization and attachment of membrane chemosensory clusters to pre-cytokinetic sites results in new-pole clusters after cytokinesis (Greenfield *et al.*, 2009; Thiem *et al.*, 2007; Thiem and Sourjik, 2008; Wang *et al.*, 2008). To test this in *R. sphaeroides*, we observed the positioning of membrane chemosensory clusters in cephalexin-treated filamentous cells. The functional YFP fusion of $CheW_3$, expressed as a genomic replacement, was used as a marker for membrane clusters (Wadhams *et al.*, 2003). Unlike *E. coli*, membrane chemosensory clusters in *R. sphaeroides* did not colocalize with pre-cytokinetic sites (as marked by FtsZ–CFP), indeed, no detectable membrane clusters were found in the vicinities of Z-rings (Fig. 3A and see below). Occasionally (21% of cells), Z-rings were not positioned at the mid- or quarter-cells, and concomitant exclusions of membrane chemosensory clusters were seen (Fig. 3A, lower panel). These results suggest that although stochastic self-assembly may participate in the positioning of membrane chemosensory clusters in *R. sphaeroides*, the final positions are not correlated with future cytokinetic sites. Indeed, the membrane clusters appear unable to localize to these sites.

The establishment of new-pole membrane chemosensory clusters

How does *R. sphaeroides* establish the bipolar localization of membrane chemosensory clusters if the clusters are not targeted to pre-cytokinetic sites? Unipolar localization of membrane chemosensory clusters (Fig. 3B and S4A) could be seen in some new-born cells, suggesting new-pole clusters form after cell division and cells eventually reach a bipolar pattern. Two possible scenarios are: (1) new-pole clusters are formed via *de novo* nucleation and assembly; (2) new-pole clusters are derived from elsewhere in the cell, with these clusters moving to the new pole. Tracking the membrane chemosensory clusters showed they are dynamic and move randomly in the membrane. Small clusters left old poles and moved along the length of the cell (Fig. 3B). The lateral movement of clusters suggests new-pole clusters can derive from lateral or even old-pole clusters, to become trapped by the curvature at the new pole (Endres, 2009; Thiem et al., 2007). Single-particle tracking showed that lateral chemosensory clusters have a diffusion coefficient D of $4.1\times10^{-3}\pm3.0\times10^{-3}$ μm^2/min, with an average velocity of 17±6 nm/min, and a maximum of ~80 nm/min. Individual lateral clusters frequently showed pauses with varied time length (mean=41.5±28.1 min, n=34 clusters; Fig. S5, A and B). However, the mean square displacement (MSD) *vs.* time interval plots of most trajectories (74%) can be fitted

with a straight line (R^2=0.97±0.03), indicating normal Brownian diffusion. The pauses could be caused by transient encounters with obstacles like cell-wall synthesis machinery.

Inhibition of protein synthesis should impede the formation of new-pole clusters if they are formed *de novo*, while new-pole clusters derived from the diffusion of existing lateral clusters should be unaffected. Control and chloramphenicol-treated cells had similar ratios of unipolar cells, 32±6% (n=424) and 30±3% (n=653), respectively. By following the fate of unipolar cells using time-lapse imaging, we found that within 100 min, 55±2% (n=197) became bipolar in the presence of chloramphenicol, comparing to 62±4% (n=82) of control cells. This difference should be much greater if new-pole clusters formed *de novo*, because there would not be sufficient mature fluorescent chemosensory proteins to form new clusters at the onset of imaging. These results indicate new-pole clusters are derived from old-pole or lateral clusters. Directional movements would not be required for the proposed old-pole/lateral clusters-derived mechanism, since random movements coupled with polar trapping will eventually redistribute clusters to the new pole.

We tested this idea by using a different approach. We followed the behavior of a chemoreceptor (McpG–GFP) in a *ΔcheW$_2$cheW$_3$* strain. In both *E. coli* and *R. sphaeroides* deletion of CheW results in diffuse chemoreceptors, somewhat more

concentrated towards the curved polar regions but without cluster formation, with clusters reforming when *cheW*$_2$*cheW*$_3$ are re-expressed (Wadhams *et al.*, 2000 and this study). We followed the cluster formation when the expression of *cheW*$_2$*cheW*$_3$ was induced by IPTG, and found that clusters first formed dispersed around the cell and the clusters then gradually moved to and accumulated at the cell poles (Fig. S6). Therefore, clustering of membrane chemosensory proteins can take place all around the cell membrane, and the resulted chemosensory clusters have a propensity to move toward and accumulate at the cell poles.

Taken together, the above results suggest that in a wild-type scenario, new-pole clusters are most likely derived from existing lateral or old-pole clusters.

FtsZ and membrane chemosensory protein clusters do not colocalize

After cell division the time taken for membrane chemosensory clusters to arrive at the new pole was very variable: from before FtsZ moved away from the new-pole (Fig. 3Bi and S4A) to after Z-ring formation (Fig. 3Biii and S4A), suggesting no direct coupling of the redistribution of FtsZ and establishment of new-pole clusters. However, FtsZ polar spots never colocalized with new-pole clusters, although

diffraction-limited images occasionally show them to be close (Fig. 3Bi, 20'). Time-lapse imaging showed that membrane chemosensory clusters move into the very tip of the new pole once FtsZ polar spots are no longer present (Fig. 3B, i and iii). Similar relative localization patterns were seen for FtsZ and membrane clusters in photoheterotrophic cells (Fig. S4B). We sought to explore whether this is just a coincidence of the timing of two independent processes. One possibility is that certain concentration of chemosensory proteins is required before a new-pole cluster can form. However, there was no obvious correlation between the amount of chemosensory proteins in the cell and the appearance of new-pole clusters or movement of small clusters from the old pole (e.g. compare Fig. 3Bi to 3Biii; Fig. S4C). This observation also argues against a purely stochastic self-assembly process in the positioning of membrane chemosensory clusters in *R. sphaeroides*.

Blocking cytokinesis, which consequently delays the redistribution of FtsZ and formation of new-poles, should accelerate the relative timing of new-pole cluster formation if there is merely a coincidence of timing (Fig. 4, schematics). If the membrane curvature of the cell pole is the main determinant for polar chemosensory cluster localization (Endres, 2009), releasing cells from cephalexin treatment should also accelerate the formation of new-pole clusters (Fig. 4, left part of the schematics). If however the presence of Z-rings/FtsZ polar spots at the forming new pole affects

the establishment of new-pole clusters, we should see a time delay (Fig. 4, right part of the schematics). Small membrane chemosensory clusters gradually moved into the new pole only after FtsZ started leaving (Fig. 4; seen in 88.6% of cells, n=88). The simplest explanation is that chemosensory clusters move from the old poles or lateral sites, diffuse around the cell, but are excluded from the developing new poles by constricting Z-rings. The completion of cytokinesis allows the laterally accumulated clusters to diffuse into the new poles. Moreover, the data support the notion that new-pole clusters are derived from existing clusters moving into the new pole.

From the above data, it seems that the Z-ring inhibits/constrains membrane chemosensory clusters from accumulating at cytokinetic sites (Fig. 3 and 4), while FtsZ polar spots might have a different effect (e.g. steric hindrance) at cell poles. Overexpression of FtsZ in *R. sphaeroides* resulted in randomly distributed spots (Fig. S7B). Close proximity of FtsZ and membrane chemosensory clusters was only observed for FtsZ spots, not for Z-rings (Fig. S7). Accordingly, membrane chemosensory clusters localized as proposed for a stochastic self-assembly pattern (i.e. the "default" pattern) in FtsZ-overexpressing cells (Fig. S7B). This observation indicates that the Z-ring (or associated factors) modifies the localization pattern of membrane chemosensory clusters in *R. sphaeroides*.

As a huge macromolecular assembly that alters the cell envelope, the

Z-ring/divisome may exclude other proteins from its vicinity. We sought to further explore this by following the dynamics of lateral chemosensory clusters relative to the Z-ring in cephalexin-treated cells. The average distance between Z-rings and their nearest lateral clusters is 324±100 nm (n=92). This result suggests a region covering ~300 nm at both sides of the Z-ring is unfavorable for the localization of membrane chemosensory clusters in *R. sphaeroides* (Fig. S5A, arrowheads; S5C).

Membrane chemosensory proteins form dynamic unit-clusters

The polar "caps" formed by membrane chemosensory proteins have been viewed as single large, static entities (Greenfield *et al.*, 2009; Ping *et al.*, 2008; Schulmeister *et al.*, 2008; Zhang *et al.*, 2007). However, our observations suggest that in *R. sphaeroides*, the polar caps are composed of smaller, dynamic clusters. The polar caps changed their shapes continuously (e.g. Fig. 3Biii) as these small clusters congregate and segregate (Fig. 5A). This suggests there may be a basic unit of membrane chemosensory proteins, and the polar caps or bigger clusters are formed from dynamic congregation–segregation of these unit-clusters (Fig. 5B, schematics). This idea is supported by quantifying the intensities of small clusters over time (Fig. 5B).

We observed similar localization patterns for chemosensory receptors McpB and McpG (Fig. S8), suggesting this is not connected to the chemosensory protein fusion used. Therefore, membrane chemosensory proteins formed independently moving dynamic unit-clusters which may have a maximum size.

To estimate the size of unit-clusters, we ranked membrane clusters in snapshots according to their intensities. The distribution of cluster intensity shows a two-phase pattern (Fig. S9A) which can be explained by a unit-cluster model (Fig. 5C), with unit-clusters growing by assembling processes (1st linear phase in Fig. S9A), with end of the linear phase representing the average size of unit-clusters. The second exponential phase represents the combination (congregation) of growing and mature unit-clusters (Fig. 5C). It should be noted that the first linear phase does not imply that the unit-clusters grow linearly, since exponential growth with a small increase rate could also result in a good linear fit. Instead, the two-phase pattern indicates the nature of dominant assembling components (e.g. oligomers or unit-clusters).

Since membrane chemosensory clusters are better separated in filamentous FtsZ-overexpressing cells, we performed intensity-ranking analyses on these cells for the average size of unit-clusters by correlating fluorescence intensity to quantitative fluorimetry data (Wilkinson *et al.*, 2011). The data suggest an average of ~1100 $CheW_3$ proteins per unit-cluster. Mapping each cluster to the intensity-ranking curve

by its localization reveals striking patterns (Fig. S9A). The first linear phase is mainly composed of lateral and new-pole clusters, while the second exponential phase is composed of new-pole and old-pole clusters (Fig. S9A). The distribution patterns suggest lateral clusters are basically unit-clusters, old-pole clusters are essentially congregations of multiple unit-clusters, and new-pole clusters can either be made of one or more unit-clusters. The average intensity of lateral clusters is ~470 counts on our camera detector (corresponding to ~920 $CheW_3$ molecules), coinciding with the plateau-like region of intensity-ranking curve (Fig. S9B, dashed circle). The intensities of larger lateral clusters bunch together around a value (Fig. S9B, solid circle) about twice of that of the plateau-like region, suggesting these larger lateral clusters were composed of two unit-clusters. The intensity-ranking curve of new-pole clusters also shows a first linear phase (Fig. S9C). The intensity value at the transition point is ~500 counts (corresponding to ~970 $CheW_3$ molecules). Taken together, the estimations of unit-cluster size from the intensity distributions of lateral and new-pole clusters in normal cells, as well as clusters in filamentous cells, suggest a value of ~920–1100 $CheW_3$ proteins per unit-cluster.

Cytoplasmic chemosensory clusters stay close to FtsZ assemblies during most of the cell cycle

The cytoplasmic chemosensory clusters are composed of homologues of the membrane clusters, and the daughter cells need to inherit both clusters on cell division to allow chemotaxis. We have shown that the cytoplasmic clusters move dynamically in *R. sphaeroides* cells with time-average positions at pre-cytokinetic sites and these clusters appear linked to chromosome movement via a ParA-like system (Roberts *et al.*, 2012; Thompson *et al.*, 2006). Consistent with this, snapshots show that cytoplasmic chemosensory clusters (marked by TlpT–YFP) were close to the Z-ring (Fig. 6A). For cells with multiple clusters, most of them (86.0%) have at least one cluster close to the Z-ring (Fig. 6B). By using the different FtsZ assemblies as indicators of cell-cycle stages, we found that the colocalization of cytoplasmic clusters and FtsZ was cell-cycle related (Fig. S10, A and B). The frequent proximity of cytoplasmic chemosensory clusters and constricting Z-rings or polar FtsZ spots (Fig. S10A, last and first cells, respectively; S10B) was unexpected, since it is believed that non-chromosome cytoplasmic cargos of ParA homologues move to the future cytokinetic sites before cytokinesis (Gerdes *et al.*, 2010; Lutkenhaus, 2012). Time-lapse imaging shows that in two-cluster cells, one cluster moved to a

pre-cytokinetic site first (Fig. 6C, white arrowhead), while another cluster stayed with the Z-ring and gradually moved to the other pre-cytokinetic site later (Fig. 6C, green arrowheads). The proximity to the Z-ring was often seen even after extensive constriction of the Z-ring (Fig. S10C, green arrowheads).

Our data suggest that cytoplasmic chemosensory clusters and FtsZ occupy similar subcellular locations, at least to within the optical resolution limit of our microscope. However, the movement of cytoplasmic clusters to the pre-cytokinetic sites before FtsZ (Fig. 6C and S10, A and C) suggests cytoplasmic clusters do not use FtsZ assemblies as anchors for positioning. The asymmetric movement of the two cytoplasmic clusters to the future midcell (Fig. 6C and S10C) is consistent with assemblies moving with chromosome segregation (Lutkenhaus, 2012), suggesting a larger role for the chromosome in this process than previously postulated. Similar spatiotemporal dynamics of cytoplasmic chemosensory clusters was seen in photoheterotrophic cells (Fig. S10D), indicating that the reorganization of the cytoplasmic membrane does not interfere with cytoplasmic chemosensory cluster positioning.

Relative positioning between MreB, FtsZ, and chemosensory clusters

The actin homologue MreB participates in the spatial regulation of different biomolecules in bacteria (Shaevitz and Gitai, 2010). The dominant models for the *in vivo* configurations of MreB cytoskeleton during the past decade are filamentous helices or rings (Shaevitz and Gitai, 2010). However, we observed circumferentially arranged GFP–MreB patches in most cells of a *R. sphaeroides* strain harboring the genomic *gfp–mreB* fusion (Fig. 7, A and B) (Slovak *et al.*, 2005), which is consistent with current studies (Domínguez-Escobar *et al.*, 2011; Garner *et al.*, 2011; Swulius and Jensen, 2012; van Teeffelen *et al.*, 2011). Since the GFP–MreB fusion is not fully functional (Slovak *et al.*, 2005), we examined the localization of MreB in a merodiploid strain containing an IPTG-inducible copy of *yfp–mreB* in addition to the native genomic *mreB* copy. Leaky expression resulted in a similar patchy pattern of MreB localization (Fig. 7, C and D).

We observed a cell cycle-specific colocalization between FtsZ and MreB. FtsZ nodes/rings and MreB colocalize at midcell until constriction, after which MreB relocalizes at future midcell before FtsZ (Fig. 7, A and B) (Slovak *et al.*, 2005). The localization patterns of the MreB ring-like arrangement and the Z-ring suggest two independent structures (Fig. 7B). MreB forms ring-like structures which colocalized

with and are dependent on the Z-ring in *C. crescentus* and *E. coli* (Aaron *et al.*, 2007; Vats and Rothfield, 2007). However, the establishment of medial ring-like arrangement of MreB seems to be independent of the Z-ring in *R. sphaeroides* (Fig. 7, A and B) (Slovak *et al.*, 2005), suggesting a novel mechanism to position MreB assemblies in this bacterium.

To explore the possible role of MreB plays in the positioning of membrane and cytoplasmic chemosensory clusters, we monitored the localizations of chemosensory clusters together with MreB. No correlation was found (Fig. 7, C and D).

Discussion

Z-ring formation

Our data show that FtsZ forms dynamic, cell cycle-dependent assemblies in *R. sphaeroides*, which can exhibit substantial reorganization during the formation of the Z-ring. The polar spots localized to the new poles immediately after cytokinesis redistribute to the midcell to initiate the formation of the Z-ring (Fig. 1 and 3Bi). These polar spots could move as single or multiple independent entities. FtsZ spots change in their intensities, numbers, and positions. Redistribution of FtsZ spots to the midcell allows the formation of Z-rings. FtsZ spatial gradients stretch out from nodes and eventually encircle the midcell plane, undergoing rearrangements and a more symmetric allocation is reached. Structures similar to FtsZ nodes have been seen in *C. crescentus* (Quardokus *et al.*, 2001), *E. coli* (Sun and Margolin, 1998), sporulating *Streptomyces coelicolor* (Willemse *et al.*, 2011), an ectosymbiotic γ-proteobacterium divides longitudinally (Leisch *et al.*, 2012), and cyanelles (cyanobacteria-like endosymbionts) (Sato *et al.*, 2009), suggesting a common mechanism for the formation of Z-rings.

One current model for Z-ring formation suggests that the Z-ring forms by the collapse of a helical structure (Ben-Yehuda and Losick, 2002; Peters *et al.*, 2007; Thanbichler and Shapiro, 2006; Thanedar and Margolin, 2004). However, less than 1% of *R. sphaeroides* cells showed the extended spiral-like structures under medium induction (up to 7.5 μM IPTG). Instead, more than 50% of *R. sphaeroides* cells had clear Z-ring precursors (Table S1). One possibility is that similar Z-ring precursors are only transiently present in other bacteria, and the helical structures may represent a relaxed Z-ring or adjacent structures. The longer cell cycle of *R. sphaeroides* increases the chance of seeing the Z-ring precursors and serves as a good model to study Z-ring development.

Another nucleation site model (Addinall and Lutkenhaus, 1996; Pichoff and Lutkenhaus, 2005) suggests the formation of Z-ring initiate at single (Addinall and Lutkenhaus, 1996) or multiple (Pichoff and Lutkenhaus, 2005) midcell sites. Bidirectional polymerizations emerging from nucleation sites produce long FtsZ polymers that associate laterally to form Z-rings. For the nucleation model to be true, the Z-ring must be composed of a few long protofilaments that grow from the nucleation sites and encircle the midcell plane. However, *in vitro* and *in vivo* data suggest that FtsZ protofilaments from diverse species are only 100 to 200 nm long (Erickson *et al.*, 2010; Li *et al.*, 2007), much shorter than the circumference of a

typical bacterium. Since the midcell node in *R. sphaeroides* contains the majority of total cellular FtsZ molecules (Table S1), further protein synthesis is not required for Z-ring formation (i.e. the relocation of polar spots and the reorganization of midcell nodes into mature Z-rings), and the Z-ring development process is reversible (Fig. S2C), we believe that the main function of midcell nodes is probably to allow reorganization/redistribution of FtsZ rather than *de novo* nucleation. Nevertheless, it is possible that the reorganization/redistribution of FtsZ may include nucleation–polymerization process taking place at the edges of the FtsZ nodes/gradients.

The positioning of membrane chemosensory clusters

Membrane chemosensory clusters accumulated at both poles, as seen in many bacterial species, with one obvious old pole and one new pole (Gestwicki *et al.*, 2000). A group of polar-flagellated γ-proteobacteria show a modified, cell cycle-dependent bipolar pattern: new-born cells have a unipolar distribution of chemosensory clusters at the old pole, and becomes bipolar as the new pole matures (Ringgaard *et al.*, 2011). Stochastic self-assembly/helical insertion (Greenfield *et al.*, 2009; Shiomi *et al.*, 2006;

Thiem and Sourjik, 2008; Wang *et al.*, 2008) and ParA homologue-mediated diffusion-and-capture (Ringgaard *et al.*, 2011) mechanisms have been proposed for the two patterns, respectively. *C. crescentus* represents an extreme with a sole unipolar localization programmed by its intrinsic asymmetry (Alley *et al.*, 1992). In *E. coli* polar clusters seem relatively dynamic, but remain at the cell poles, while new clusters localized laterally at pre-cytokinetic sites, appearing tightly localized (Thiem *et al.*, 2007). The situation in *R. sphaeroides* seems very different: the polar clusters appear to be formed from a number of smaller clusters, which appear to freely diffuse as large complexes in the lateral membrane with some polar retention. The lateral clusters are not static, and there is no accumulation at pre-cytokinetic sites. Indeed, the clusters appear to be excluded from the vicinities of Z-rings. A periodic pattern seen in cephalexin-treated filamentous cells is probably determined by a synergistic action of stochastic self-assembly and an exclusive effect associated (directly or indirectly) with the Z-ring. Taken together, stochastic self-assembly, diffusion-and-capture, and a Z-ring-associated exclusive effect may coordinate to generate the spatiotemporal dynamics of membrane chemosensory clusters in *R. sphaeroides*.

Although FtsZ spots seem to only have a steric-hindrance effect on the localization of membrane chemosensory clusters, the Z-ring/divisome may create an

environment with different physicochemical properties in its vicinity (Lopez-Montero *et al.*, 2012), preventing membrane chemosensory clusters to localize in the Z-ring vicinity.

Dynamic unit-clusters of membrane chemosensory proteins

While much of the previous fluorescence and cryo-electron microscopy data has suggested the membrane chemosensory proteins form massive polar clusters, our data suggest that in *R. sphaeroides* there is an optimum cluster size and these smaller clusters are free to diffuse, but tend to accumulate at the poles. Similar congregation–segregation process (Thiem *et al.*, 2007) and pattern of intensity-ranking plots (Ping *et al.*, 2008) can be seen in *E. coli*. Quantification of fluorescence intensities from lateral clusters in normal and filamentous cells suggests an average cluster size of about 1000 $CheW_3$ molecules. As quantitative fluorimetry data suggest an average of 8700±260 $CheW_3$ molecules/cell (with the majority present in membrane clusters) (Wilkinson *et al.*, 2011), this suggests 6–8 clusters per unit cell, which correlates well with the numbers seen in normal and filamentous cells when clusters were segregated (Fig. 3A and 5A).

The clustering of the chemosensory proteins into large quaternary complexes may be important for the high level of sensitivity and gain in the bacterial chemosensory pathway (Bray *et al.*, 1998; Gestwicki and Kiessling, 2002), but recent data suggest that signaling works through signaling teams that are smaller in size (Hansen *et al.*, 2010). The size (upper limit) of clusters could be jointly determined by intracluster forces that hold constituting subunits and the nature of surrounding environments (Endres, 2009). It is likely that intercluster interactions create transient, unstable couplings between unit-clusters. With the same number of constituting proteins, several unit-clusters may generate better digital signals than a single huge cluster, hence improved signaling fidelity (Suzuki, 2012).

Recent data have suggested that when *R. sphaeroides* grows photoheterotrophically, rather than producing invaginations tightly connected to the inner membrane, the intracytoplasmic photosynthetic membranes bud from a limited number of sites on the inner membrane to form intracellular vesicles (Tucker *et al.*, 2010). This is supported by our data as the behavior of FtsZ and membrane chemosensory clusters in photoheterotrophic and aerobic cells are similar, suggests a relatively similar inner membrane organization.

The partitioning of cytoplasmic chemosensory clusters

Previous work has shown that the cytoplasmic chemosensory cluster segregates using a ParA-like protein, PpfA, which localizes to the chromosome surface, suggesting a plasmid-like segregation system (Roberts *et al.*, 2012; Thompson *et al.*, 2006). Dynamic oscillation of ParA homologues has been suggested to constantly adjust the inter-cargo distance and equi-partition cargos (Gerdes *et al.*, 2010; Lutkenhaus, 2012). One feature of such mechanisms is a symmetric distribution of cargos. The cytoplasmic chemosensory clusters and FtsZ often colocalize to the same midcell region over a large portion of the cell cycle, but the two duplicated clusters move to daughter cells independently. We do not see equi-partitioning of the cytoplasmic chemosensory clusters, which may reflect the absence of oscillations seen for PpfA (Roberts *et al.*, 2012) and suggests asymmetrically segregating chromosomes (i.e. only one copy of the duplicated chromosomes is translocated across the cell) could act as the anchor/carrier.

The cell cycle-specific colocalization between MreB and FtsZ is different in *R. sphaeroides* compared to *C. crescentus* and *E. coli* (Aaron *et al.*, 2007; Vats and

Rothfield, 2007): the medial ring-like arrangement of MreB forms before and are independent of the formation of the Z-ring (Fig. 7, A and B) (Slovak *et al.*, 2005). This observation suggests that there are diverse interacting modes in the homologous cytoskeletal networks in different bacteria. Moreover, it is possible that MreB assemblies at pre-cytokinetic sites may assist in the development process of the Z-ring. Although previous studies (Shiomi *et al.*, 2006; Thiem *et al.*, 2007) suggest MreB may not be involved in the positioning of membrane chemosensory clusters, the distinct localization pattern of MreB prompted us to investigate the role of MreB in the positioning of membrane and cytoplasmic chemosensory clusters in *R. sphaeroides*. However, no apparent correlation was found.

Taken together these data show that very different mechanisms are employed to ensure daughter cells inherit two homologous protein complexes generating chemosensory signals, both required for chemotaxis, one relying on the diffusing of large protein complexes and polar trapping, the other is partitioned using the segregating daughter chromosomes. Unlike previous observations, the membrane clusters form unit complexes which diffuse in the cell and neither chemosensory cluster has positioning linked directly to the positioning of FtsZ or MreB through the cell cycle. The data also show a detailed pattern of FtsZ positioning through the *R.*

sphaeroides cell cycle, with polar spots moving to midcell to produce nodes from which the Z-ring develops. Therefore, our study provides new perspectives on the complete life cycle of the Z-ring and the dynamic nature of chemosensory clusters.

Experimental procedures

Bacterial strains and growth conditions

The strains and plasmids used in this study were constructed as described before (Porter *et al.*, 2007) and are listed in Table S2. All *R. sphaeroides* strains were derived from WS8N and grown in succinate medium with antibiotics at 30 °C. When appropriate, the antibiotics nalidixic acid and kanamycin were used at 25 μg ml^{-1}. All experiments were performed with log-phase aerobic or photoheterotrophic (illuminated with light at 10 W/m^2) cells. *E. coli* XL1-Blue was used for cloning. *E. coli* strain S17-1λ*pir* was used for conjugal DNA transfer into *R. sphaeroides* (Porter *et al.*, 2007). For inducing filamentation, cells were (1) treated with 2.5 μg ml^{-1} cephalexin for 3.5 h or (2) induced with 250 μM IPTG overnight before imaging. To inhibit protein synthesis, chloramphenicol was added to the bacterial culture at a final concentration of 50 μg ml^{-1} (Romagnoli *et al.*, 2002). For time-lapse imaging, cells pre-treated with chloramphenicol for 90 min were laid on agarose pads pre-soaked in medium containing chloramphenicol.

Microscopy and image analysis

Cells were immobilized on 0.8% agarose pads in succinate medium and observed using a DeltaVision platform (Applied Precision) equipped with a 100 × 1.4 NA Plan-Apochromat objective and a Coolsnap HQ camera. The live-cell filter set was used. Imaging settings were carefully selected to avoid saturation of the camera, and were kept constant for similar samples. To optimize the accuracy of protein colocalization, each z-stack was acquired with one channel immediately followed by another. Cells were optically sectioned into multiple slices spacing 80–120 nm and deconvolved using the DeltaVision softWoRx 4.0.0 restoration system. Cells were imaged at 25°C.

Images are, unless specified, maximal projections of z-stacks. However, for quantification of intensity, sum projections were used. Background intensity was subtracted. Quantification and analysis were performed in ImageJ (rsbweb.nih.gov/ij). Brightness and contrast adjustment, when performed, was applied uniformly to whole images. For single-particle tracking, distance measurement and colocalization categorizing, the centroid (for spherical chemosensory clusters), center of mass (for irregular-shaped chemosensory clusters), and edges (for FtsZ assemblies) were used.

Cell Counter (http://rsbweb.nih.gov/ij/plugins/cell-counter.html) was used as a plug-in for ImageJ to count and categorize assemblies and cells.

Fluorimetry

Strain JPA1418 cells were collected and resuspended in succinate medium to give a wide range of cell concentrations. Resuspended cells were transferred to black, clear-bottom 96-well plates (Corning) and fluorescence readings were taken using appropriate YFP filters on a FLUOstar Optima fluorescence plate reader (BMG LABTECH) with a gain setting of 2200. A cellular autofluorescence baseline was calculated using wild-type WS8N cells and subtracted from the measured values. For protein copy number quantification, fluorescence signal was compared to that obtained from known quantities of purified YFP, resuspended in the same number of WS8N cells (Wilkinson *et al.*, 2011).

Acknowledgments

We thank Micron Oxford for help with microscopy. SWC was supported with an EPA Cephalosporin Scholarship by the Linacre College (Oxford, U.K.) and a Scholarship for Studying Abroad by Ministry of Education (Taiwan, R.O.C.). MCL was supported by a Royal Society University Research Fellowship. This work was supported by BBSRC.

References

Aaron, M., Charbon, G., Lam, H., Schwarz, H., Vollmer, W., and Jacobs-Wagner, C. (2007) The tubulin homologue FtsZ contributes to cell elongation by guiding cell wall precursor synthesis in *Caulobacter crescentus*. *Mol Microbiol* **64:** 938–952.

Adams, D.W., and Errington, J. (2009) Bacterial cell division: assembly, maintenance and disassembly of the Z ring. *Nat Rev Microbiol* **7:** 642–653.

Addinall, S.G., and Lutkenhaus, J. (1996) FtsZ-spirals and -arcs determine the shape of the invaginating septa in some mutants of *Escherichia coli*. *Mol Microbiol* **22:** 231–237.

Alley, M.R., Maddock, J.R., and Shapiro, L. (1992) Polar localization of a bacterial chemoreceptor. *Genes Dev* **6:** 825–836.

Ben-Yehuda, S., and Losick, R. (2002) Asymmetric cell division in *B. subtilis* involves a spiral-like intermediate of the cytokinetic protein FtsZ. *Cell* **109:** 257–266.

Bray, D., Levin, M.D., and Morton-Firth, C.J. (1998) Receptor clustering as a cellular mechanism to control sensitivity. *Nature* **393:** 85–88.

Briegel, A., Ortega, D.R., Tocheva, E.I., Wuichet, K., Li, Z., Chen, S., Müller, A.,

Iancu, C.V., Murphy, G.E., Dobro, M.J., Zhulin, I.B., and Jensen, G.J. (2009) Universal architecture of bacterial chemoreceptor arrays. *Proc Natl Acad Sci USA* **106:** 17181–17186.

de Boer, P.A. (2010) Advances in understanding *E. coli* cell fission. *Curr Opin Microbiol* **13:** 730–737.

Domínguez-Escobar, J., Chastanet, A., Crevenna, A.H., Fromion, V., Wedlich-Söldner, R., and Carballido-López, R. (2011) Processive movement of MreB-associated cell wall biosynthetic complexes in bacteria. *Science* **333:** 225–228.

Endres, R.G. (2009) Polar chemoreceptor clustering by coupled trimers of dimers. *Biophys J* **96:** 453–463.

Erickson, H.P., Anderson, D.E., and Osawa, M. (2010) FtsZ in bacterial cytokinesis: cytoskeleton and force generator all in one. *Microbiol Mol Biol Rev* **74:** 504–528.

Fu, G., Huang, T., Buss, J., Coltharp, C., Hensel, Z., and Xiao, J. (2010) *In vivo* structure of the *E. coli* FtsZ-ring revealed by photoactivated localization microscopy (PALM). *PLoS One* **5:** e12680.

Garner, E.C., Bernard, R., Wang, W., Zhuang, X., Rudner, D.Z., and Mitchison, T. (2011) Coupled, circumferential motions of the cell wall synthesis machinery and MreB filaments in *B. subtilis*. *Science* **333:** 222–225.

Gerdes, K., Howard, M., and Szardenings, F. (2010) Pushing and pulling in

prokaryotic DNA segregation. *Cell* **141:** 927–942.

Gestwicki, J.E., and Kiessling, L.L. (2002) Inter-receptor communication through arrays of bacterial chemoreceptors. *Nature* **415:** 81–84.

Gestwicki, J.E., Lamanna, A.C., Harshey, R.M., McCarter, L.L., Kiessling, L.L., and Adler, J. (2000) Evolutionary conservation of methyl-accepting chemotaxis protein location in bacteria and archaea. *J Bacteriol* **182:** 6499–6502.

Gitai, Z. (2005) The new bacterial cell biology: moving parts and subcellular architecture. *Cell* **120:** 577–586.

Govindarajan, S., Nevo-Dinur, K., and Amster-Choder, O. (2012) Compartmentalization and spatiotemporal organization of macromolecules in bacteria. *FEMS Microbiol Rev* **36:** 1005–1022.

Greenfield, D., McEvoy, A.L., Shroff, H., Crooks, G.E., Wingreen, N.S., Betzig, E., and Liphardt, J. (2009) Self-organization of the *Escherichia coli* chemotaxis network imaged with super-resolution light microscopy. *PLoS Biol* **7:** e1000137.

Hansen, C.H., Sourjik, V., and Wingreen, N.S. (2010) A dynamic-signaling-team model for chemotaxis receptors in *Escherichia coli*. *Proc Natl Acad Sci USA* **107:** 17170–17175.

Hallez, R., Bellefontaine, A.F., Letesson, J.J., and De Bolle, X. (2004) Morphological and functional asymmetry in alpha-proteobacteria. *Trends Microbiol* **12:** 361–365.

Jain, I.H., Vijayan, V., and O'Shea, E.K. (2012) Spatial ordering of chromosomes enhances the fidelity of chromosome partitioning in cyanobacteria. *Proc Natl Acad Sci USA* **109:** 13638–13643.

Lan, G., Daniels, B.R., Dobrowsky, T.M., Wirtz, D., and Sun, S.X. (2009) Condensation of FtsZ filaments can drive bacterial cell division. *Proc Natl Acad Sci USA* **106:** 121–126.

Leisch, N., Verheul, J., Heindl, N.R., Gruber-Vodicka, H.R., Pende, N., den Blaauwen, T., and Bulgheresi, S. (2012) Growth in width and FtsZ ring longitudinal positioning in a gammaproteobacterial symbiont. *Curr Biol* **22:** R831–832.

Li, Z., Trimble, M.J., Brun, Y.V., and Jensen, G.J. (2007) The structure of FtsZ filaments in vivo suggests a force-generating role in cell division. *EMBO J* **26:** 4694–4708.

Lopez-Montero, I., Mateos-Gil, P., Sferrazza, M., Navajas, P.L., Rivas, G., Velez, M., and Monroy, F. (2012) Active membrane viscoelasticity by the bacterial FtsZ-division protein. *Langmuir* **28:** 4744–4753.

Lutkenhaus, J. (2012) The ParA/MinD family puts things in their place. *Trends Microbiol* **20:** 411–418.

Macara, I.G., and Mili, S. (2008) Polarity and differential inheritance–universal attributes of life? *Cell* **135:** 801–812.

Mackenzie, C., Eraso, J.M., Choudhary, M., Roh, J.H., Zeng, X., Bruscella, P., Puskás, Á., and Kaplan, S. (2007) Postgenomic adventures with *Rhodobacter sphaeroides*. *Annu Rev Microbiol* **61:** 283–307.

Niederman, R.A. (2006) Structure, function and formation of bacterial intracytoplasmic membranes. In *Complex Intracellular Structures in Prokaryotes*. Shively, J. (ed). Berlin/Heidelberg: Springer, pp. 193–227.

Niederman, R.A. (2010) Eukaryotic behaviour of a prokaryotic energy-transducing membrane: fully detached vesicular organelles arise by budding from the *Rhodobacter sphaeroides* intracytoplasmic photosynthetic membrane. *Mol Microbiol* **76:** 803–805.

Peters, P.C., Migocki, M.D., Thoni, C., and Harry, E.J. (2007) A new assembly pathway for the cytokinetic Z ring from a dynamic helical structure in vegetatively growing cells of *Bacillus subtilis*. *Mol Microbiol* **64:** 487–499.

Pichoff, S., and Lutkenhaus, J. (2005) Tethering the Z ring to the membrane through a conserved membrane targeting sequence in FtsA. *Mol Microbiol* **55:** 1722–1734.

Ping, L., Weiner, B., and Kleckner, N. (2008) Tsr-GFP accumulates linearly with time at cell poles, and can be used to differentiate 'old' versus 'new' poles, in *Escherichia coli*. *Mol Microbiol* **69:** 1427–1438.

Porter, S.L., Wadhams, G.H., and Armitage, J.P. (2007) *In vivo* and *in vitro* analysis of

the *Rhodobacter sphaeroides* chemotaxis signaling complexes. *Methods Enzymol* **423:** 392–413.

Porter, S.L., Wadhams, G.H., and Armitage, J.P. (2008) *Rhodobacter sphaeroides*: complexity in chemotactic signalling. *Trends Microbiol* **16:** 251–260.

Porter, S.L., Wadhams, G.H., and Armitage, J.P. (2011) Signal processing in complex chemotaxis pathways. *Nat Rev Microbiol* **9:** 153–165.

Quardokus, E.M., Din, N., and Brun, Y.V. (2001) Cell cycle and positional constraints on FtsZ localization and the initiation of cell division in *Caulobacter crescentus*. *Mol Microbiol* **39:** 949–959.

Ringgaard, S., Schirner, K., Davis, B.M., and Waldor, M.K. (2011) A family of ParA-like ATPases promotes cell pole maturation by facilitating polar localization of chemotaxis proteins. *Genes Dev* **25:** 1544–1555.

Roberts, M.A.J., Wadhams, G.H., Hadfield, K.A., Tickner, S., and Armitage, J.P. (2012) ParA-like protein uses nonspecific chromosomal DNA binding to partition protein complexes. *Proc Natl Acad Sci USA* **109:** 6698–6703.

Romagnoli, S., Packer, H.L., and Armitage, J.P. (2002) Tactic responses to oxygen in the phototrophic bacterium *Rhodobacter sphaeroides* WS8N. *J Bacteriol* **184:** 5590–5598.

Rudner, D.Z., and Losick, R. (2010) Protein subcellular localization in bacteria. *Cold*

Spring Harb Perspect Biol **2:** a000307.

Sato, M., Mogi, Y., Nishikawa, T., Miyamura, S., Nagumo, T., and Kawano, S. (2009) The dynamic surface of dividing cyanelles and ultrastructure of the region directly below the surface in *Cyanophora paradoxa*. *Planta* **229:** 781–791.

Schulmeister, S., Ruttorf, M., Thiem, S., Kentner, D., Lebiedz, D., and Sourjik, V. (2008) Protein exchange dynamics at chemoreceptor clusters in *Escherichia coli*. *Proc Natl Acad Sci USAA* **105:** 6403–6408.

Shaevitz, J.W., and Gitai, Z. (2010) The structure and function of bacterial actin homologs. *Cold Spring Harb Perspect Biol* **2:** a000364.

Shiomi, D., Yoshimoto, M., Homma, M., and Kawagishi, I. (2006) Helical distribution of the bacterial chemoreceptor via colocalization with the Sec protein translocation machinery. *Mol Microbiol* **60:** 894–906.

Slovak, P.M., Wadhams, G.H., and Armitage, J.P. (2005) Localization of MreB in *Rhodobacter sphaeroides* under conditions causing changes in cell shape and membrane structure. *J Bacteriol* **187:** 54–64.

Sourjik, V., and Armitage, J.P. (2010) Spatial organization in bacterial chemotaxis. *EMBO J* **29:** 2724–2733.

Sourjik, V., and Wingreen, N.S. (2012) Responding to chemical gradients: bacterial chemotaxis. *Curr Opin Cell Biol* **24:** 262–268.

Specht, M., Dempwolff, F., Schätzle, S., Thomann, R., and Waidner, B. (2013) Localization of FtsZ in *Helicobacter pylori* and consequences for cell division. *J Bacteriol* **195:** 1411–1420.

Strauss, M.P., Liew, A.T., Turnbull, L., Whitchurch, C.B., Monahan, L.G., and Harry, E.J. (2012) 3D-SIM super resolution microscopy reveals a bead-like arrangement for FtsZ and the division machinery: implications for triggering cytokinesis. *PLoS Biol* **10:** e1001389.

Sun, Q., and Margolin, W. (1998) FtsZ dynamics during the division cycle of live *Escherichia coli* cells. *J Bacteriol* **180:** 2050–2056.

Suzuki, K.G. (2012) Lipid rafts generate digital-like signal transduction in cell plasma membranes. *Biotechnol J* **7:** 753–761.

Swulius, M.T., and Jensen, G.J. (2012) The helical MreB cytoskeleton in *Escherichia coli* MC1000/pLE7 is an artifact of the N-terminal yellow fluorescent protein tag. *J Bacteriol* **194:** 6382–6386.

Thanbichler, M., and Shapiro, L. (2006) MipZ, a spatial regulator coordinating chromosome segregation with cell division in *Caulobacter*. *Cell* **126:** 147–162.

Thanedar, S., and Margolin, W. (2004) FtsZ exhibits rapid movement and oscillation waves in helix-like patterns in *Escherichia coli*. *Curr Biol* **14:** 1167–1173.

Thiem, S., Kentner, D., and Sourjik, V. (2007) Positioning of chemosensory clusters

in *E. coli* and its relation to cell division. *EMBO J* **26:** 1615–1623.

Thiem, S., and Sourjik, V. (2008) Stochastic assembly of chemoreceptor clusters in *Escherichia coli*. *Mol Microbiol* **68:** 1228–1236.

Thompson, S.R., Wadhams, G.H., and Armitage, J.P. (2006) The positioning of cytoplasmic protein clusters in bacteria. *Proc Natl Acad Sci USA* **103:** 8209–8214.

Tucker, J.D., Siebert, C.A., Escalante, M., Adams, P.G., Olsen, J.D., Otto, C., Stokes, D.L., and Hunter, C.N. (2010) Membrane invagination in *Rhodobacter sphaeroides* is initiated at curved regions of the cytoplasmic membrane, then forms both budded and fully detached spherical vesicles. *Mol Microbiol* **76:** 833–847.

van Teeffelen, S., Wang, S., Furchtgott, L., Huang, K.C., Wingreen, N.S., Shaevitz, J.W., and Gitai, Z. (2011) The bacterial actin MreB rotates, and rotation depends on cell-wall assembly. *Proc Natl Acad Sci USA* **108:** 15822–15827.

Vats, P., and Rothfield, L. (2007) Duplication and segregation of the actin (MreB) cytoskeleton during the prokaryotic cell cycle. *Proc Natl Acad Sci USA* **104:** 17795–17800.

Wadhams, G.H., Martin, A.C., and Armitage, J.P. (2000) Identification and localization of a methyl-accepting chemotaxis protein in *Rhodobacter sphaeroides*. *Mol Microbiol* **36:** 1222–1233.

Wadhams, G.H., Warren, A.V., Martin, A.C., and Armitage, J.P. (2003) Targeting of

two signal transduction pathways to different regions of the bacterial cell. *Mol Microbiol* **50:** 763–770.

Wang, H., Wingreen, N.S., and Mukhopadhyay, R. (2008) Self-organized periodicity of protein clusters in growing bacteria. *Phys Rev Lett* **101:** 218101.

Wilkinson, D.A., Chacko, S.J., Vénien-Bryan, C., Wadhams, G.H., and Armitage, J.P. (2011) Regulation of flagellum number by FliA and FlgM and role in biofilm formation by *Rhodobacter sphaeroides*. *J Bacteriol* **193:** 4010–4014.

Willemse, J., Borst, J.W., de Waal, E., Bisseling, T., and van Wezel, G.P. (2011) Positive control of cell division: FtsZ is recruited by SsgB during sporulation of *Streptomyces*. *Genes Dev* **25:** 89–99.

Yamaichi, Y., Bruckner, R., Ringgaard, S., Möll, A., Cameron, D.E., Briegel, A., *et al.* (2012) A multidomain hub anchors the chromosome segregation and chemotactic machinery to the bacterial pole. *Genes Dev* **26:** 2348–2360.

Zhang, P., Khursigara, C.M., Hartnell, L.M., and Subramaniam, S. (2007) Direct visualization of *Escherichia coli* chemotaxis receptor arrays using cryo-electron microscopy. *Proc Natl Acad Sci USA* **104:** 3777–3781.

Figure Legends

Fig. 1. The development process of the Z-ring.

A. Time-lapse images of the cell cycle stage-specific localization of FtsZ in *R. sphaeroides*. A midcell band (a ring in 3D) constricts into a denser band with smaller radius. The completion of septation results in two FtsZ spots at the new poles. Red: FtsZ–YFP; blue: differential interference contrast (DIC). Numbers: minutes of observation.

B. Z-ring precursors. (i) Polar FtsZ–YFP spots move to the future cytokinetic sites and fluorescence signals extend from the midcell nodes. (ii) Time-lapse images of the midcell showing the FtsZ spatial gradient (dashed arrows) between two midcell nodes. The longitudinal axis of the cell is perpendicular to the dashed arrows.

C. Fluctuations of FtsZ–YFP distribution along the precursor and early Z-ring. The fluorescence intensity profiles (upper panel) across the Z-ring precursors (yellow dashed box) are shown along with their corresponding time-lapse frames.

D. A pathway for Z-ring formation. Schematics depict the typical patterns in this pathway. The fluorescence intensity profiles across the midcell sections (yellow dashed box) for actual fluorescence images with the corresponding patterns are shown.

The horizontal and vertical axes are the same as in C. After moving from the new poles, the midcell nodes reorganize and FtsZ spatial gradients extend and encircle the midcell plane. A cell could have more than one midcell node.

Scale bars: 1 μm.

Fig. 2. Time-lapse images showing the spatiotemporal dynamics of FtsZ spots and Z-ring precursors. Red: FtsZ–YFP; blue: DIC. Numbers: minutes. Scale bars: 1 μm.

A. FtsZ spots change positions. Yellow arrowheads: polar spots. White arrowheads: midcell spots.

B. FtsZ spots are gradually positioned at the midcell. Two spots integrate into a single midcell node (10' to 20') which then separate into two nodes (30'). These two nodes are properly positioned at a plane perpendicular to the longitudinal axis of the cell, results in a perpendicular Z-ring (50').

Fig. 3. Spatiotemporal dynamics of membrane chemosensory clusters relative to FtsZ in *R. sphaeroides*. Green: YFP–$CheW_3$; red: FtsZ–CFP; blue: DIC. Scale bars: 1 μm.

A. Localizations of the Z-ring and membrane chemosensory clusters in

cephalexin-treated cells. Images show that the Z-ring and lateral membrane clusters do not colocalize. Arrowheads: positions of Z-rings.

B. (i) FtsZ and membrane clusters do not colocalize at the new pole. Arrowheads: a membrane cluster moves into the new pole. (ii and iii) Small clusters can move away from the old poles toward the new poles (arrowheads). Numbers: minutes.

Fig. 4. The positions of the membrane chemosensory cluster relative to FtsZ in cells released from cephalexin treatment. Green: YFP–$CheW_3$; red: FtsZ–CFP; blue: DIC. Red arrowheads: FtsZ assemblies. Dashed and solid green arrowheads: zones without and with detectable membrane clusters, respectively. Numbers: minutes. Schematic: possible scenarios of membrane cluster formation at the new pole. Left compartment: If membrane curvature is the ultimate cue for new-pole targeting of the membrane cluster, releasing the cells from cephalexin treatment should result in colocalization of FtsZ and membrane clusters at the new pole once the typical membrane curvature has formed for a stochastic process (i.e. the membrane cluster will move into and stay at the polar region in the presence of FtsZ). Right compartment: In another scenario, the presence of FtsZ at the new pole affects the polar localization of membrane clusters. Scale bars: 1 μm.

Fig. 5. The membrane clusters are dynamic and might operate as unit-clusters.

A. Time-lapse images of YFP–$CheW_3$ demonstrating that the polar "cap" is composed of several smaller clusters (arrowheads) which congregate and segregate continuously. Green: YFP–$CheW_3$; red: FtsZ–CFP; blue: DIC. Numbers: minutes. Scale bar: 1 μm.

B. The intensities of two YFP–$CheW_3$ clusters (filled arrowheads in A) were monitored over time and the ratios between them are shown. The mean autocorrelation value (x_{t+1}/x_t) is given. If membrane clusters operate as unit-clusters, the intensity ratios should keep constant after congregation–segregation (schematic).

C. A model for the formation of unit-clusters (shaded; corresponding to the 1st phase in Fig. S8A; thin arrows) and congregation of unit-clusters (2nd phase in Fig. S8A; thick arrows). Each spherical represents an oligomer of chemosensory proteins.

Fig. 6. The positions of the cytoplasmic chemosensory cluster relative to FtsZ during the cell cycle. Red, FtsZ–CFP; green, cytoplasmic clusters marked by TlpT–YFP; blue: DIC. Numbers: minutes. Scale bars: 1 μm.

A. The position of the cytoplasmic cluster in a single-cluster cell. The cluster is in proximity of the cytoplasmic membrane and adjacent to the Z-ring. Right image: the

3D reconstruction viewed from a different angle (rotated 60°).

B. The positions of the cytoplasmic cluster in a two-cluster cell.

C. A two-cluster cell released from cephalexin treatment. Here, one cluster moves to future midcell first (white arrowhead), while another stays with the Z-ring at least till constriction (green arrowheads). Red arrowheads: Z-rings.

Fig. 7. Relative positioning between MreB and FtsZ or chemosensory clusters in *R. sphaeroides*. Scale bars: 1 μm.

A. MreB and FtsZ colocalize at the midcell. Green: GFP–MreB; red: FtsZ–RFP; blue: DIC. Arrowheads: yellow, polar FtsZ spots; white, FtsZ spots presumably moving toward the midcell; blue, midcell FtsZ node. Gray scale image: 3D reconstruction of subcellular localization of GFP–MreB viewed from a different angle for one cell (rotated 130°; white arrow).

B. MreB (green) and FtsZ (red) form independent structures that partially colocalize at the midcell. Upper panel: MreB assemblies are highly dynamic, moving around the cell (or assembling–disassembling) with an average midcell localization. The Z-ring (30') matured from a precursor (0'). Lower panel: Individual z-sections for FtsZ and MreB structures. The first image is a maximum projection.

C. The relative positioning of MreB (red) and membrane chemosensory clusters (green) in cells with different localization patterns of chemosensory clusters: (i) unipolar; (ii) quasi-bipolar; (iii) bipolar.

D. The relative positioning of MreB (red) and cytoplasmic chemosensory clusters (green) in cells with different localization patterns of chemosensory clusters: (i) single midcell cluster; (ii) single polar cluster; (iii) two-cluster.

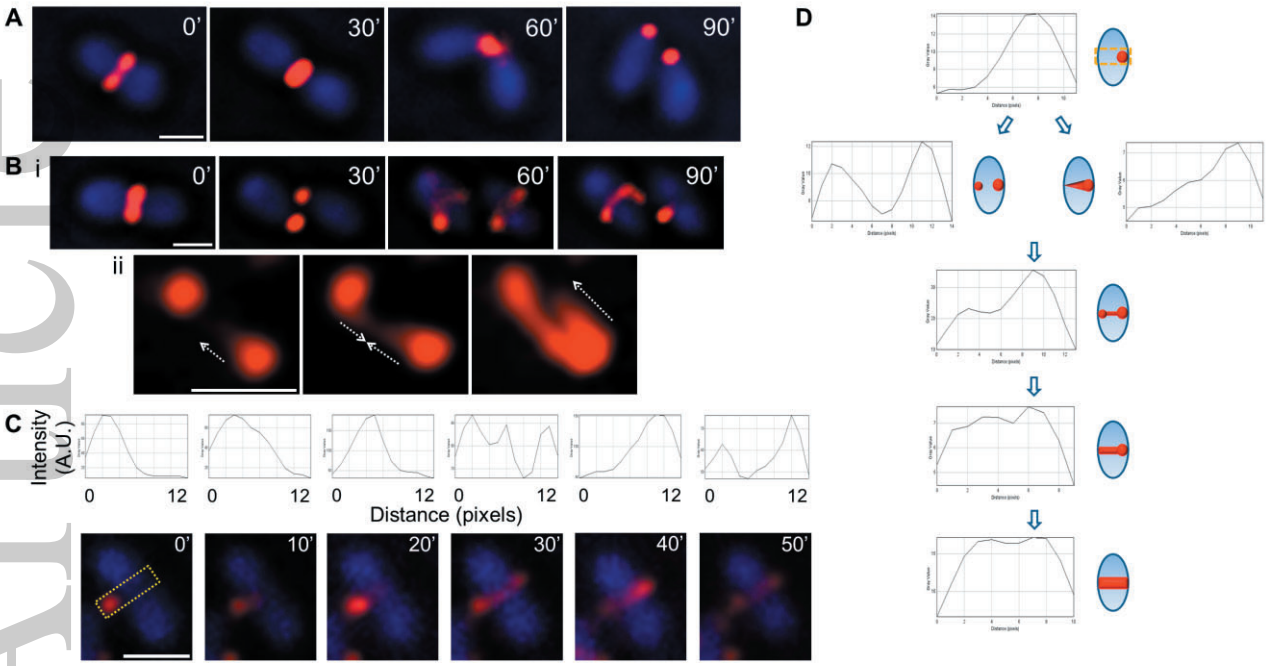

mmi_12366_f1.tif

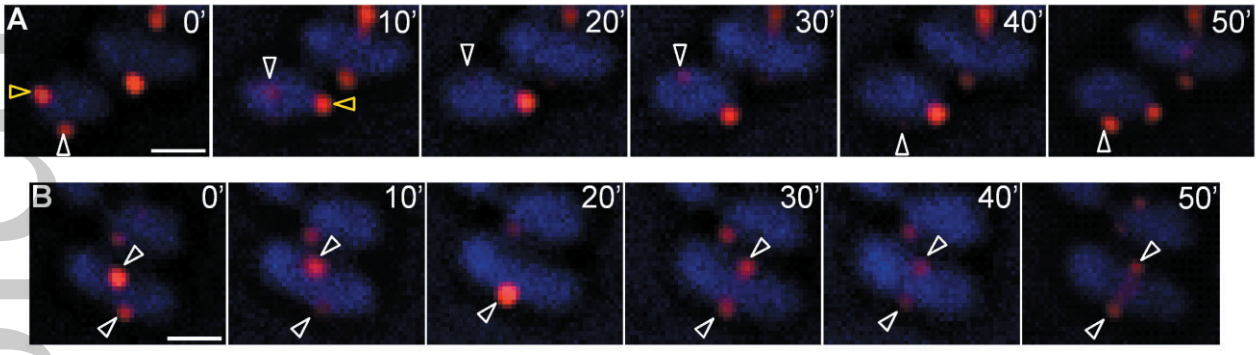

mmi_12366_f2.tif

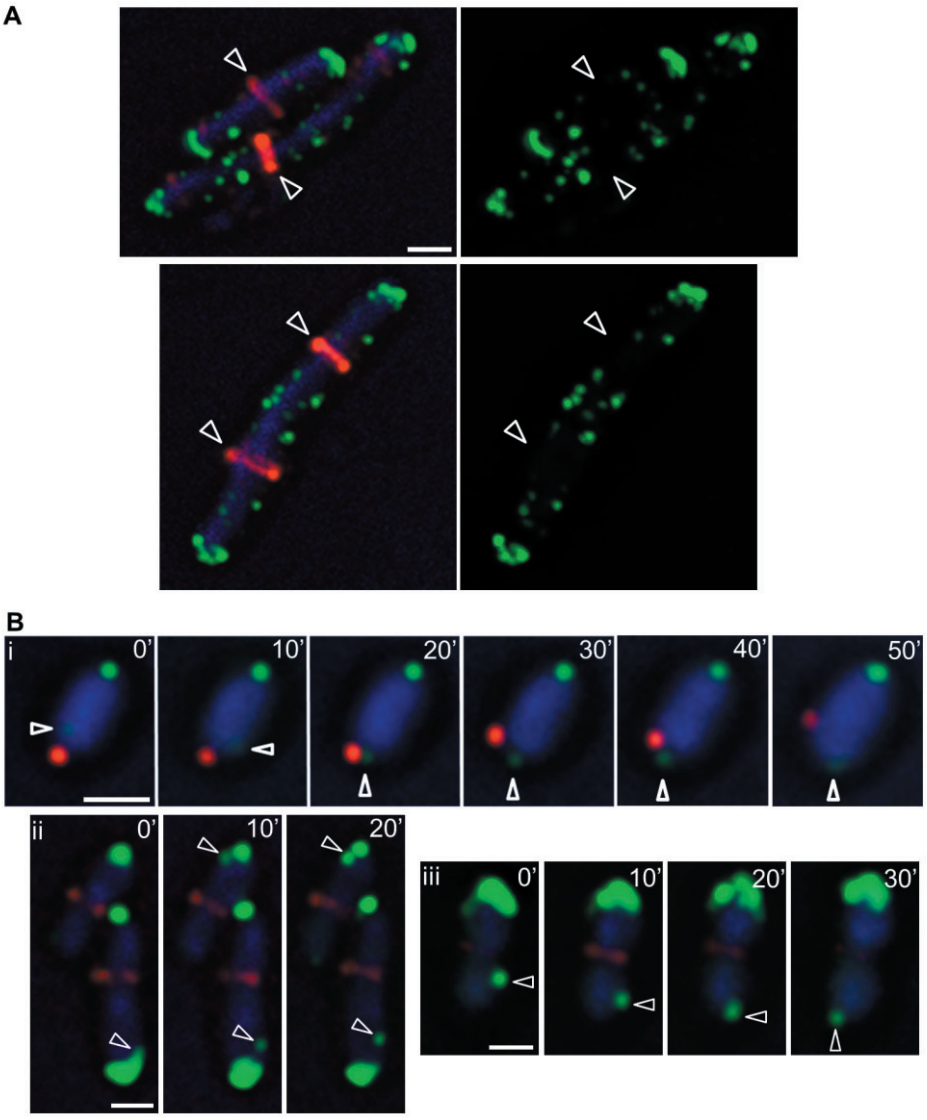

mmi_12366_f3.tif

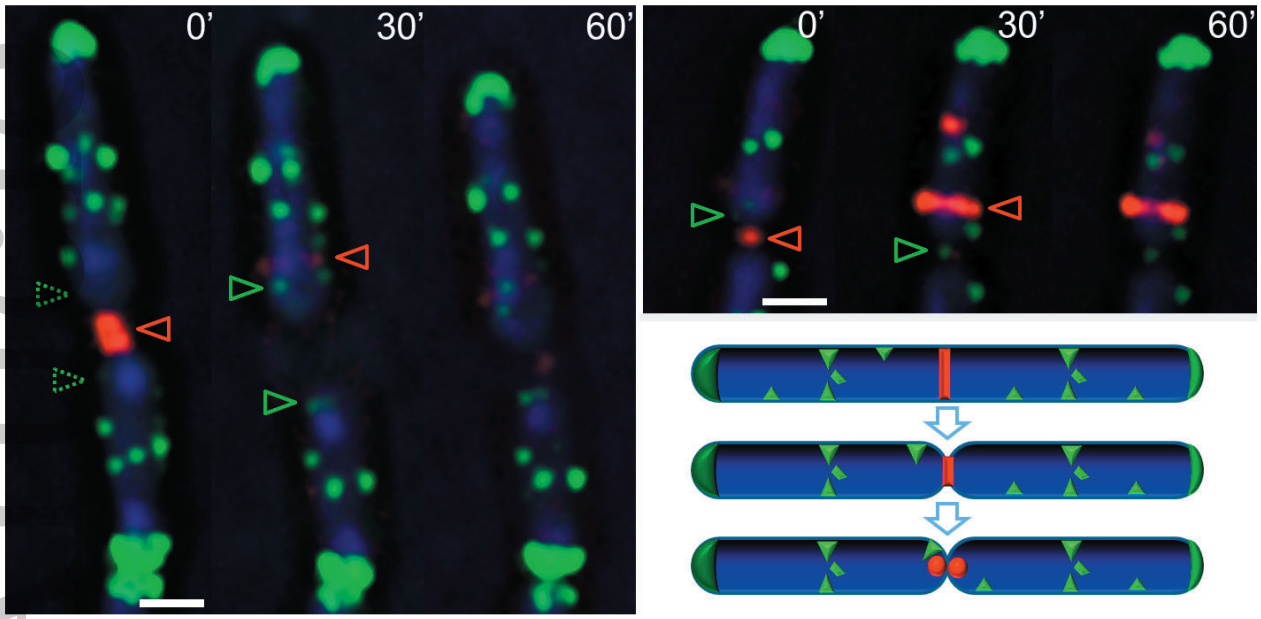

mmi_12366_f4.tif

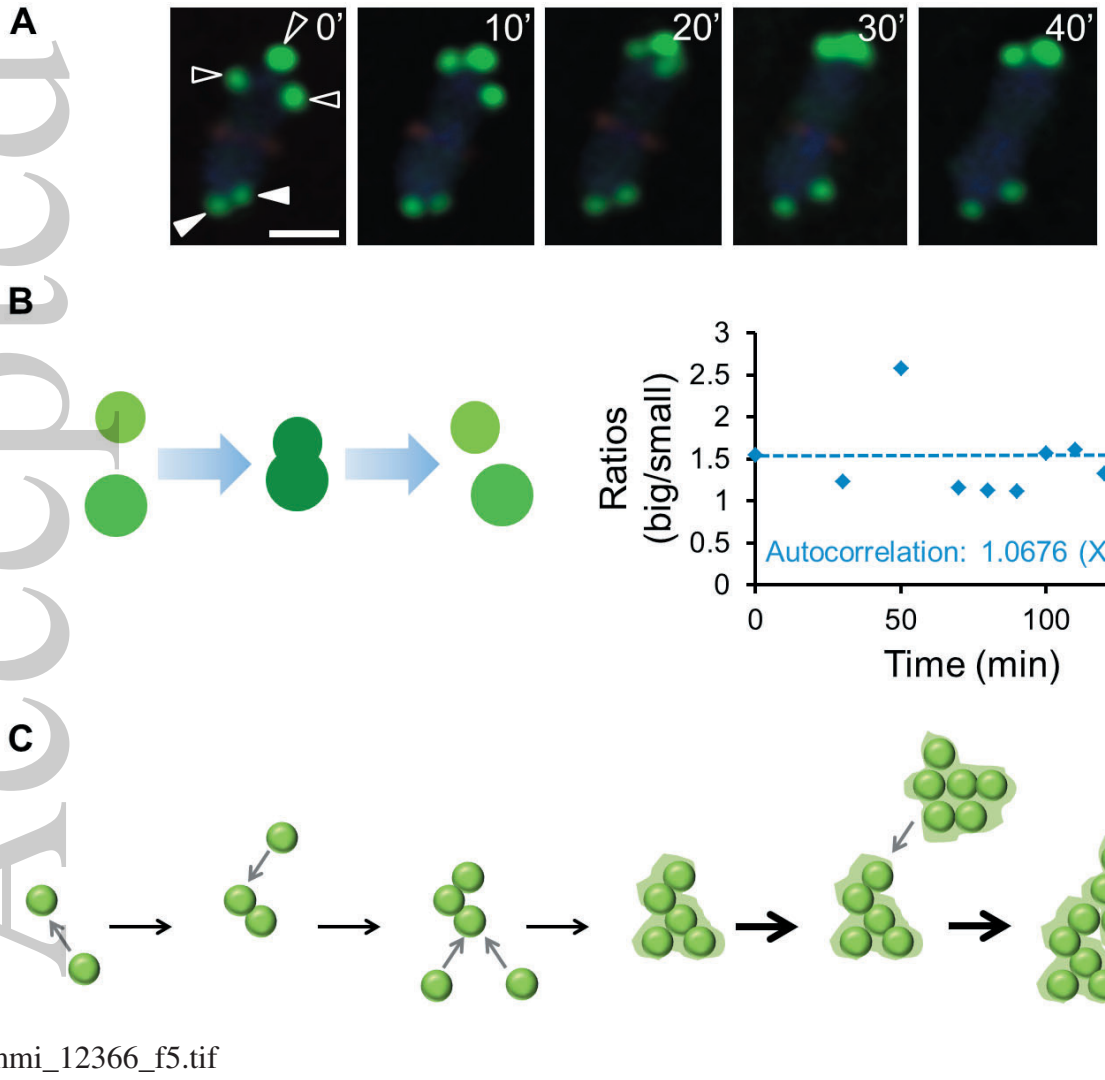

mmi_12366_f5.tif

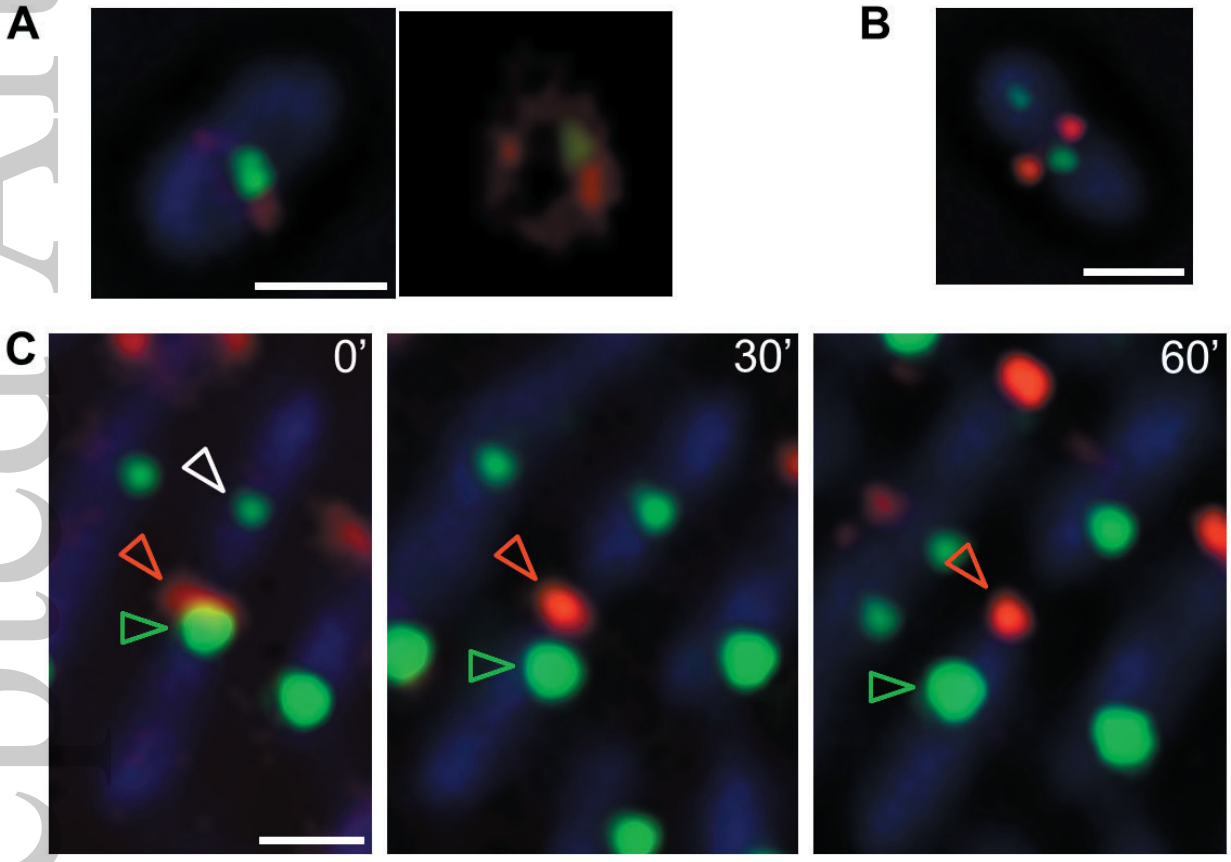

mmi_12366_f6.tif

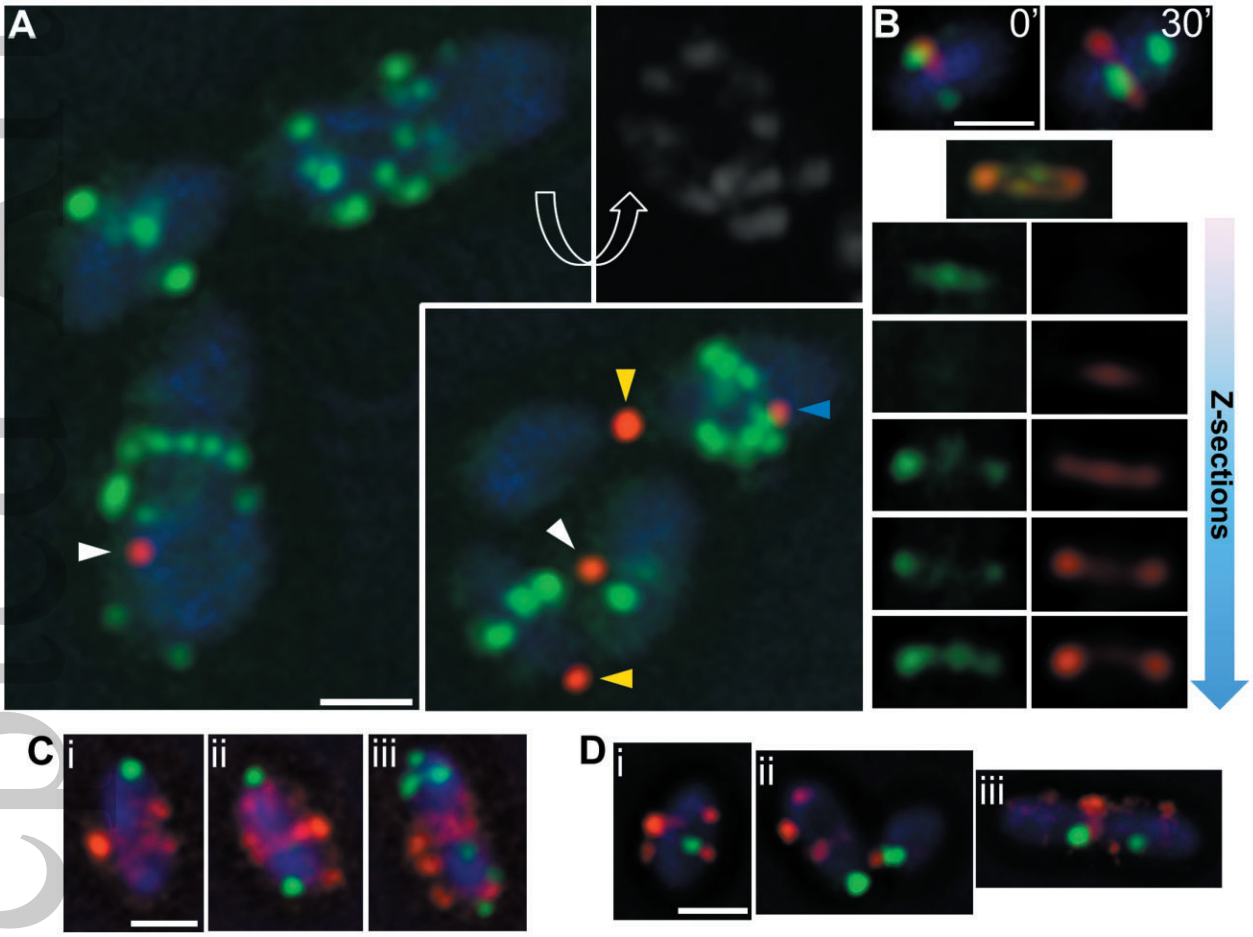

mmi_12366_f7.tif